Journal of Alloys and Compounds 500 (2010) 138–143

Contents lists available at ScienceDirect

Journal of Alloys and Compounds

journal homepage: www.elsevier.com/locate/jallcom

Effect of manganese inclusion on structural, optical and electrical properties of ZnO thin films

A.U. Ubale*, V.P. Deshpande

Thin Film Physics Laboratory, Department of Physics, Government Vidarbha Institute of Science and Humanities, VMV Road, Amravati 444 604, India

ARTICLE INFO

Article history:
Received 8 December 2009
Received in revised form 23 March 2010
Accepted 1 April 2010
Available online 8 April 2010

Keywords:
Thin films
Optical properties
Electrical properties

ABSTRACT

ZnO has become promising versatile member in semiconductor technology due to its well-known performance in electronics, optics and photonics. In present investigation we have reported the impact of manganese incorporation on electrical optical and structural properties of spray deposited ZnO thin films. The study of X-ray diffraction suggests that the films are nanocrystalline in nature having hexagonal wurtzite type crystal structure. The electrical resistivity measurement shows films are semiconducting and it decreases with increase in doping percentage. Optical absorption studies show that the band-gap energy is decreased from 3.45 to 2.64 eV as the doping percentage was increased from 0 to 5 at.%. The scanning electron micrographs (SEM) of doped ZnO thin films shows network of nanotubes. The H_2S sensing behaviour of films is also investigated.

1. Introduction

Oxide semiconductor films have been extensively investigated and have received considerable attention in recent years due to their attractive properties such as low toxicity, high conductivity, high transmittance in visible region, and high infrared reflectance and distinguish performance in electronics, optics and photonics [1,2]. In contrast to nonoxide semiconductors, the oxide semiconductors have many advantages. Their wide band gap makes them transparent and also suitable for applications with short wavelength. They can be easily grown at low temperature even on a plastic substrate and are ecologically secure and long lasting besides being near to the ground cost. ZnO is a semiconductor material of II–VI compound of the periodic table whose ionicity resides at the border line between covalent and ionic semiconductor. Zinc oxide films have found extensive applications in heterojunction solar cells [3,4], gas sensors [5,6], varistors [7], a phosphor for color displays [8], heat mirrors [9], piezoelectric devices [10] and multilayer photo-thermal conversion systems [11], light emitting diodes (LEDs), laser diodes (LDs) [12,13], etc. The large exciton binding energy of 60 meV and wide band-gap energy of 3.33 eV at room temperature make ZnO a promising photonic material for applications such as light emitting diodes, laser diodes and UV photodiodes [14–18]. In addition, ZnO is one of the environmentally friendly bio-safe and biocompatible material, and can be used directly for biomedical applications without coating materials, and the impurity-doped ZnO nanocrystals emitting visible light are expected to be appropriate materials for flat panel displays, florescence labels for biological imaging, and so on [19]. Due to these versatile properties and wide applications of the ZnO, it is one of the most important materials for future research and applications.

Low resistive zinc oxide films have been achieved by doping with different group III elements like aluminum, boron, gallium and indium or with group VII elements like fluorine [20]. The awareness in doping ZnO is to discover possibility of tailoring its electrical, magnetic and optical properties [21–25]. The doping of transition metal elements into ZnO offers a feasible means of fine tuning the band gap to make use as UV detector and light emitters. Many techniques can be employed to deposit of ZnO thin films which includes molecular beam epitaxy (MBE) [26], thermal evaporation [27], rf sputtering [28,29], chemical vapor deposition [30–32], pulsed laser deposition [33–35], magnetron sputtering [36], sol–gel technique [37], spray pyrolysis [38,39], etc. Out of these techniques, chemical spray pyrolysis technique has received attention due to its simplicity and consequent economics aspect as it does not require high vacuum equipments, and another attractive point is the possibility of production of large-area films. It has several advantages such as simplicity, safety and low cost of the equipments and raw materials. In this technique, a starting solution containing a soluble salt of the cation of interest is sprayed by means of a nozzle assisted by a carrier gas over a hot substrate. When the fine droplets arrive at the substrate, thermal decomposition takes place to produce desired thin film. The quality and the physical properties of the films depend on the various process parameters, such as substrate temperature, molar concentration of the starting solution,

* Corresponding author. Tel.: +91 721 2531706; fax: +91 721 2531705.
E-mail address: ashokuu@yahoo.com (A.U. Ubale).

0925-8388/$ – see front matter © 2010 Elsevier B.V. All rights reserved.
doi:10.1016/j.jallcom.2010.04.004

Table 1
Optimized preparative parameters for deposition of Mn doped ZnO thin film.

Spray parameter	Optimum value
Concentration of Zn-acetate	0.1 M
Concentration Mn-acetate	0.1 M
Solvent	Distilled water
Substrate temperature	573 ± 5 K
Carrier gas	Compressed air
Solution flow rate	8 cm^3 min^{-1}
Nozzle	Glass
Nozzle substrate distance	25 cm

spray rate, type and pressure of the carrier gas and the geometric characteristics of the spray system.

Recently, much attention has been paid to optical, electrical and magnetic properties of nanostructured semiconductor thin films doped with functional impurities because of their potential applications in optoelectronic devices [40–44]. Since ZnO has wide band-gap energy, its nanocrystals are appropriate host materials for the doping of transition metal ions and rare-earth which are optically and magnetically active [45–48]. ZnO thin films have been prepared and studied for various p-type and n-type doping elements like Al, Ba, Ga, In, Cu, I, Co, Li, Mn, etc. But no significant data were published on optical, structural and electrical properties of ZnO films doped with Mn. The main objective of the present work was focused on the structural, optical, and electrical properties of Mn doped ZnO thin films doped with Mn grown by spray pyrolysis.

2. Experimental

2.1. Preparation

Mn doped zinc oxide films were deposited on to glass substrates by means of spray pyrolysis technique. The glass substrates on which the films were prepared placed on a surface of substrate heater. The atomization of the solution into a spray of fine droplets was carried out by spray nozzle, with the help of compressed air as carrier gas. During the course of spray, the substrate temperature was monitored using a chromel alumel thermocouple, and was kept constant at 573 ± 5 K. To achieve Mn-doping, Mn-acetate was added to the solution of zinc acetate. The Mn doping was varied from 0 to 5 at.% in ZnO thin film. The resulting solution was sprayed on to preheated substrate. To optimize the different deposition parameters such as substrate temperature, spray rate, concentration of zinc acetate, several trials were done. It was found that films deposited at temperature lower than 573 K are powdery and less adhesive. The optimum concentration of zinc acetate solution was found to be 0.1 M. The film deposited at higher concentration (>0.1 M) are nonuniform and powdery. It was observed that for lower spray rate films are uniform and mirror like. The optimized spray rate was found 8 cm^3 min^{-1}. All these optimized preparative parameters are given in Table 1.

2.2. Characterization

Characterization is an essential part of all investigations. Before designing any device, a complete and deeper understanding of the properties and performance of material must be known. In present work the characterization was done to investigate electrical, optical and structural properties. The thickness of film was determined by weight difference method and it is of the order of ~130 nm. The structural characterization of Mn doped ZnO films was carried out by analyzing the X-ray diffraction pattern obtained using Philips PW 1710 diffractometer using Cu-Kα radiation of wavelength 1.5405 Å. The two point dc probe method of dark electrical resistivity is used to study the variation of resistivity with temperature. Optical absorption spectra of the films were recorded using an UV-VIS-NIR spectrophotometer model Hitachi-330. The wavelength range was between 300 and 800 nm. This data was further analyzed for estimation of band-gap energy of film. The film morphology was examined using a (JSM 61000) scanning electron microscope (SEM).

3. Results and discussion

3.1. XRD studies

The crystal structure and orientation of Mn-doped ZnO thin films were investigated from X-ray diffraction patterns (Fig. 1). It is found that films are nanocrystalline in nature having hexagonal

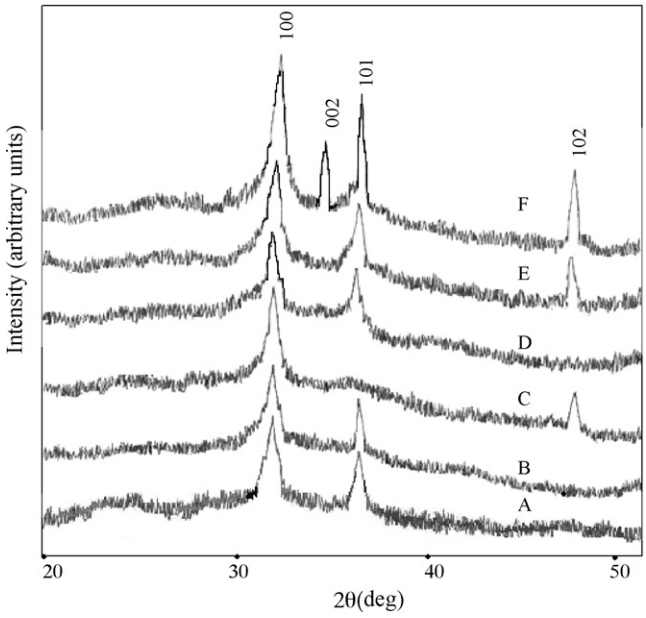

Fig. 1. XRD patterns of Mn doped ZnO thin films (A) 0 at.%, (B) 1 at.%, (C) 2 at.%, (D) 3 at.%, (E) 4 at.%, and (F) 5 at.%.

type structure. XRD Pattern shows that all the doped films have (1 0 0) as the preferred orientation. The XRD spectra was changed due to doping, the peak intensity of (1 0 0), (1 0 1) and (1 0 2) crystal plane was increased remarkably. The Mn inclusion into the ZnO improves the orientation, as the peak intensity increases with doping %. The comparison of XRD data with the standard JCPDS data is shown in Table 2. For 5 at.% doping of Mn the spectra shows (0 0 2) peak, which means that the orientation perpendicular *c*-axis appears. However the (1 0 2) orientation is observed for higher doping %. Its evident from the XRD data that there are no extra peaks due to manganese metal, manganese oxides or any zinc manganese phase, indicating that the as-synthesized samples are single phase. The Mn ion was understood to have substituted the Zn site without changing the wurtzite structure. It may be due to small doping percentage of Mn in ZnO. The average crystallite size, *d* was estimated

Table 2
Comparison of observed crystallographic data of ZnO thin film with standard JCPDS (79-0208) card.

Sample	Mn doping (at.%)	*h k l*	Standard data		Observed data	
			2θ (degree)	*d* (Å)	2θ (degree)	*d* (Å)
A	0	100	31.619	2.827	31.589	2.820
		101	36.100	2.486	36.157	2.481
B	1	100	31.619	2.827	31.518	2.831
		101	36.100	2.486	36.102	2.500
C	2	100	31.619	2.827	31.645	2.812
		102	47.367	1.917	47.320	1.919
D	3	100	31.619	2.827	31.606	2.822
		101	36.100	2.486	36.134	2.486
E	4	100	31.619	2.827	31.627	2.825
		101	36.100	2.486	36.098	2.497
		102	47.367	1.917	47.360	1.976
F	5	100	31.619	2.827	31.680	2.823
		002	34.335	2.609	34.378	2.612
		101	36.100	2.486	36.112	2.481
		102	47.367	1.917	47.388	1.929

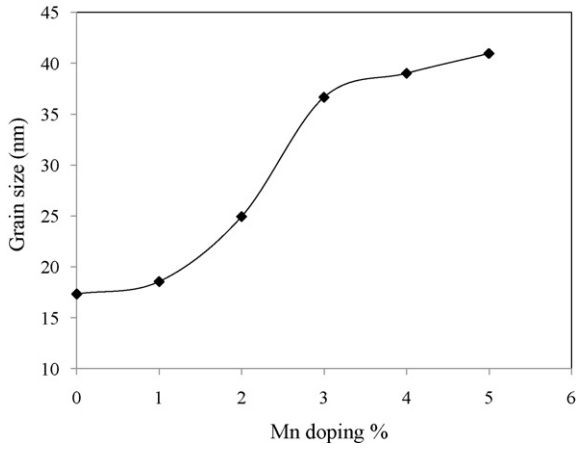

Fig. 2. Variation of grain size (nm) with Mn doping (%) in ZnO thin films.

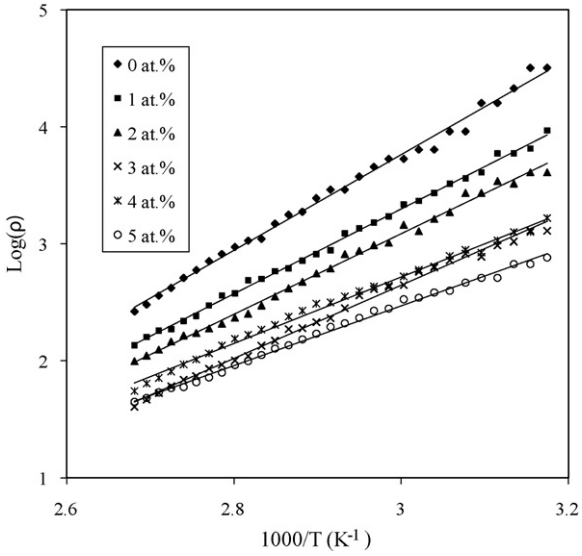

Fig. 3. Variation of $\log(\rho)$ vs. $1/T \times 10^3$ (K^{-1}) for Mn doped ZnO films.

by using the by Debye-Scherrer's equation [49],

$$d = \frac{\lambda}{\beta \cos\theta} \quad (1)$$

In this equation, λ represent the wavelength of the X-ray radiation, β the full width at half maximum of the diffraction pick (in radians) and Θ the maximum scatter angle. Fig. 2 shows variation of grain size of ZnO with Mn-doping %. It is found that as the doping percentage increases, grain size increases from 17 to 41 nm.

3.2. Electrical properties

The two point dc-probe method for measuring the dark resistivity shows that the film prepared are semiconductor in nature. It was observed the resistivity decreases as the Mn doping percentage increases from 0 to 5 at.%. Fig. 3 shows the variation of logarithm of electrical resistivity ($\log\rho$) with reciprocal of temperature ($1/T$) for ZnO films having different doing percentage of dopant Mn. The decrease in resistivity is due to rise in the free electron concentration with Mn-inclusion in the ZnO lattice which increases the donar concentration. The low electrical resistivity in TCO's (transparent conductive oxide) films is due to high electron concentration comes from the impurities doping and from non-stoichiometry. The Mn belong to third group element, Mn^{2+} atoms will substitute zinc and

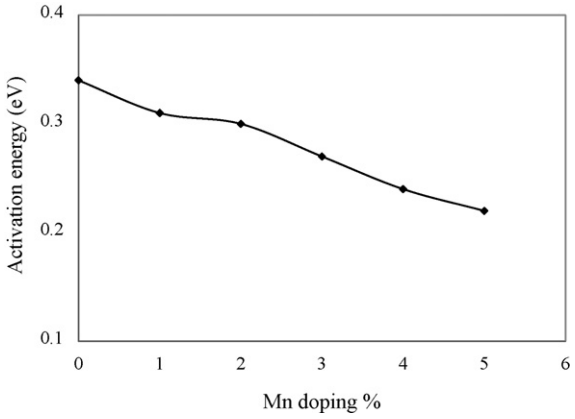

Fig. 4. Variation of activation energy of ZnO with Mn doping %.

act as donor. The mechanism of doping with transition elements ($3d$-ions) such as Mn^{2+} depends on the substitution between Mn and oxygen vacancies. The resistivity of film was decreased from 2.64×10^2 to 0.45×10^2 Ω-cm as Mn doping in ZnO is increased from 0 to 5 at.% concentration. The thermal activation energy was calculated using the relation,

$$\rho = \rho_0 \exp\left(\frac{E_0}{KT}\right) \quad (2)$$

where ρ is resistivity at temperature T, ρ_0 is a constant; K is Boltzmann constant. The activation energy decreased from 0.34 to 0.22 eV as the percentage of Mn doping increases from 0 to 5 at.%. The variation of activation energy with Mn doping is shown in Fig. 4.

3.3. Optical properties

The optical absorption of the undoped ZnO and Mn doped ZnO thin films was determined by the spectrophotometer within the wavelength range of 300–800 nm. The typical room temperature absorbance spectra for undoped ZnO and different concentration of Mn doped ZnO are shown in Fig. 5. It shows the variation of relative absorbance (αt), t being the film thickness, with wavelength. The nature of optical transition involved for the nanocrystalline film, can be determined by considering the dependence of α on $h\nu$ using equation,

$$\alpha = \frac{A(h\nu - E_g)^n}{h\nu}, \quad (3)$$

where $h\upsilon$ is the photon energy, E_g is the band-gap energy, A and n are constants. For allowed direct transitions $n = 1/2$ and for allowed indirect transitions $n = 2$. The plots of $(\alpha h\nu)^2$ vs. $h\nu$ were shown in Fig. 6. The band gap E_g is determined by extrapolation of the linear portion of the plot to the energy exists. It is found that the band-gap energy is decreased from 3.45 to 2.64 eV as the doping percentage is varied from 0 to 5 at.%. We observed red shift in the band gap due to Mn doping in ZnO. The decrease in E_g for increasing Mn content may also be due to the s-d and p-d interactions giving rise to band gap bowing and it has been theoretically explained using second-order perturbation theory [50].

3.4. Thermo emf studies

The temperature difference between the ends of sample causes transport of carriers from hot to cold end and thus create field which gives thermal voltage. The variation of thermo emf with temperature difference for Mn doped ZnO films is shown in Fig. 7. From thermo emf measurement it was observed that the polarity of thermally generated voltage at the hot end is positive indicating that

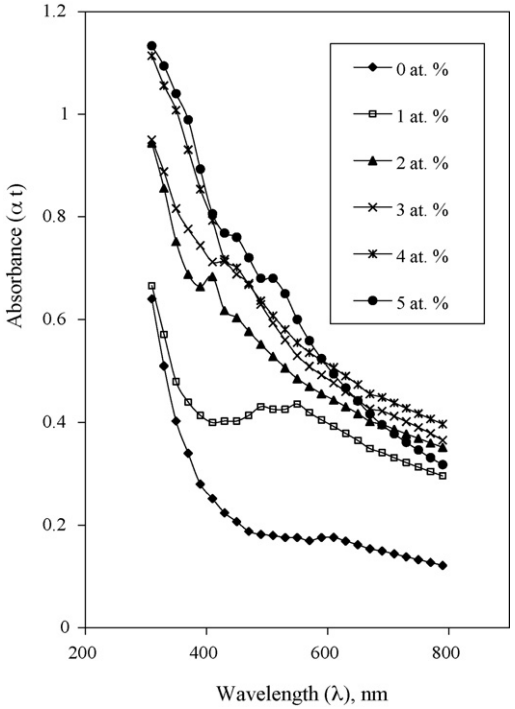

Fig. 5. Plot of optical absorption (αt) vs. wavelength for Mn doped ZnO films.

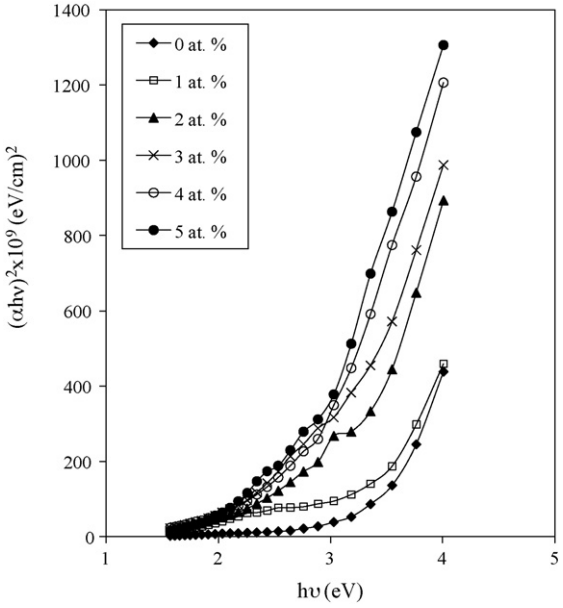

Fig. 6. Plot of $(\alpha h\nu)^2$ vs. $h\nu$ for ZnO films having different Mn doping percentage.

films are of n-type. Increase in thermo emf with increasing doping percentage is attributed to the decrease in electrical resistivity caused by increase in grain size and carrier concentration.

3.5. SEM studies

Fig. 8 shows the scanning electron micrographs for undoped i.e. 0 at.% doped and Mn-doped ZnO thin film. It shows that the surface roughness of the film increases with doping. The noodle like structure is observed which may be future application like nanotubes. This structure becomes more prominent in doped film. A dopant can influence the growth kinetics during deposition process which affects the grain structure. These images reveal that the high density nanowires or nanotubes were aligned to the substrate to form net like structure. All the nanotubes are exhibiting a smooth surface throughout their lengths. Some interesting morphologies, flower-like ZnO nanostructures composed of ZnO nanorods, were seen in sample (A) and (D). It was clearly seen that the several nanorods are accumulated on a single nucleation site through their bases and make the flower-shaped morphology.

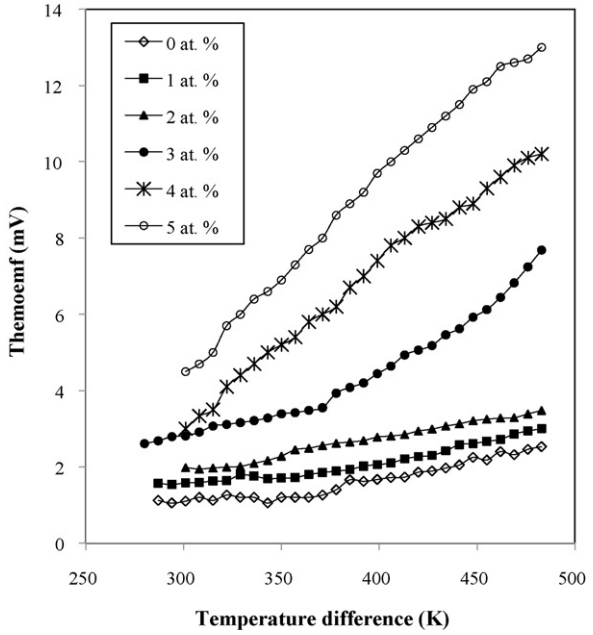

Fig. 7. Variation of thermo emf with temperature difference for Mn doped ZnO thin films.

3.6. H_2S gas sensing

The easiest way to study the gas sensor is by simply measuring the DC resistance of the sensing element as a function of temperature with and without gas in the surrounding atmosphere. Nanostructured materials have been widely used to produce new semiconductor gas sensors because of enhanced activity provided by their inherently large surface area [51]. The gas sensitivity (s) is defined as the ratio of the resistance of the sensor in air (R_{air}) to that in the test gas (R_{gas}). For gas sensing characterizations, the sensor elements were placed in a 1000 cm^3 gas chamber. Doping of ZnO produces the electronic defects and increases the influence of oxygen on the conductivity of the films. Thus an oxygen ion acts as a trap to electrons from the bulk of the films. The electrons are taken from ionized donors through conduction band and the density of majority charge carriers at the gas–solid interface is reduced. This leads to the formation of a potential barrier for electrons with increasing the oxygen ions density on the surface the further oxygen adsorption is inhibited. Thus at the junctions between ZnO grains, the depletion layer and potential barrier affects the value the electrical resistivity. This value is strongly dependent on the concentration of adsorbed oxygen ions of the surface. Fig. 9 shows H_2S gas sensitivity plots for Mn doped ZnO thin films for 400 ppm gas concentration. The sensitivity increases with increase in the operating temperature showing maximum in the temperature range 355–361 K. As doping percentage increases the sensing temperature decreases slightly towards lower temperature side. The maximum sensitivity increases from 2.1 to 6.37 with Mn doping. It is well known that sensitivity of the sensor strongly depends

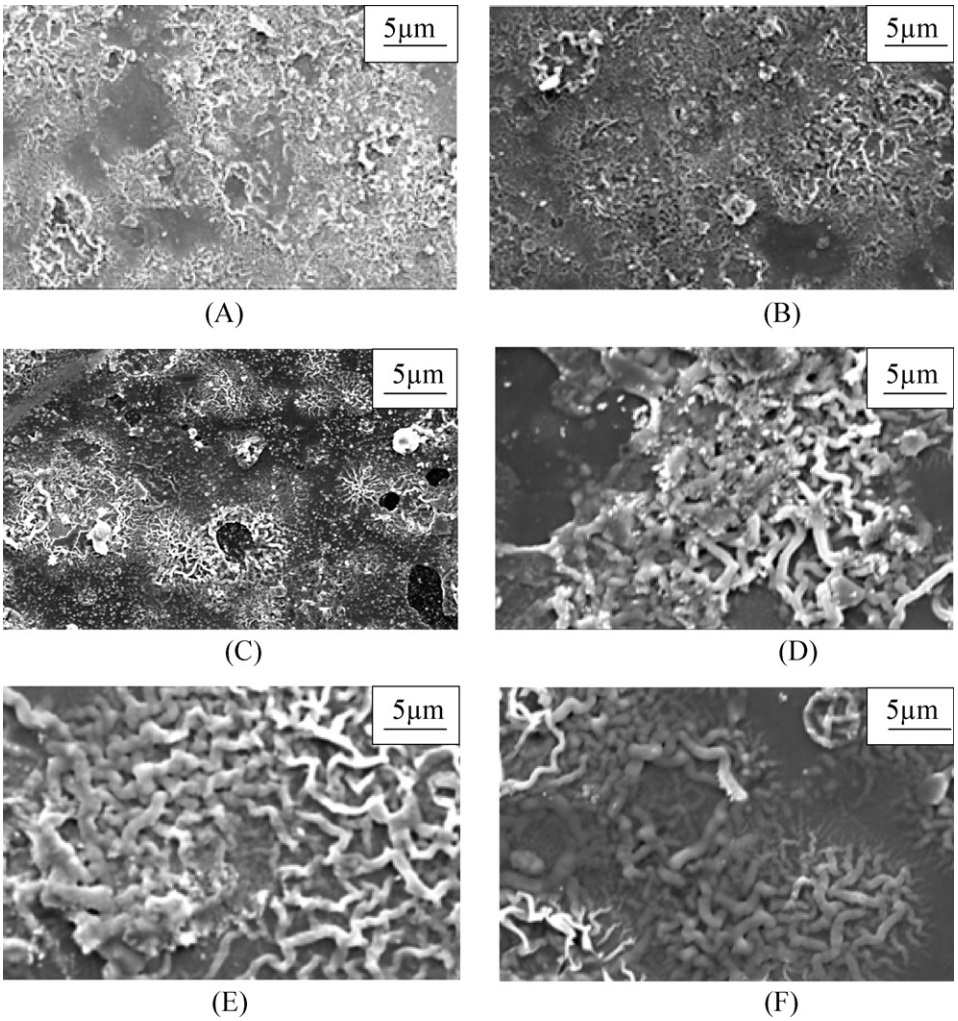

Fig. 8. SEM micrograph of Mn doped ZnO thin films: (A) 0 at.%, (B) 1 at.%, (C) 2 at.%, (D) 3 at.%, (E) 4 at.% and (F) 5 at.% doping.

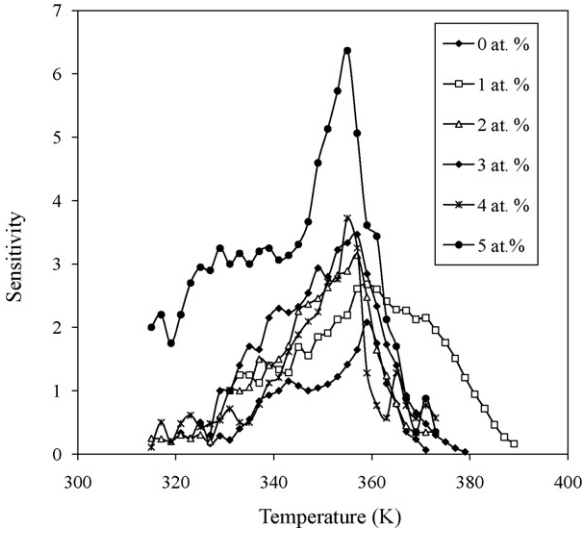

Fig. 9. Plots of H_2S gas sensitivity for Mn doped ZnO thin films.

on the grain dimensions of the sensing material. This is probably due to Mn doping the grain surface improved which provides more area for gas absorption, as the nanotubes are well developed with Mn doping % in ZnO.

4. Conclusions

The good quality Mn doped ZnO thin films were deposited on to glass substrate with the help of spray pyrolysis technique. The impact of manganese inclusion on structural, optical and electrical properties was studied. Mn doped ZnO thin films are nanocrystalline in nature with hexagonal type crystal structure having (1 0 0) as a preferred orientation. The electrical resistivity of ZnO film decreases with Mn doping percentage. The activation energy is changed from 0.34 to 0.24 eV with Mn doping. The optical absorption studies shows that band-gap energy is decreased from 3.45 to 2.64 eV as the doping is increased from 0 to 5 at.%. The rise in thermo emf with doping percentage is attributed to decrease in electrical resistivity. The SEM studies show the noodle like structure which may be future application in nanotubes. This structure becomes more prominent in Mn doped ZnO film. The sensing behaviour for H_2S shows more sensitivity for higher Mn doping % with little decrease in operating temperature.

Acknowledgement

The authors are thankful to University Grants Commission, WRO, Pune (India), for financial support under the project (No. F47-258/2007).

References

[1] X.T. Zhang, Y.C. Liu, J.Y. Zhang, Y.M. Lu, D.Z. Shen, X.W. Fan, X.G. Kong, J. Crystal Growth 254 (2003) 80.
[2] P. Sharma, K. Sreenivas, K.V. Rao, J. Appl. Phys. 93 (2003) 3963.
[3] H. Kobayashi, H. Mori, T. Ishida, Y. Nakato, J. Appl. Phys. 77 (1995) 1301.
[4] K. Elmer, J. Phys. D: Appl. Phys. R17 (2000) 33.
[5] F.C. Lin, Y. Takao, Y. Shimizu, M. Egshiro, J. Am. Ceram. Soc. 78 (1999) 2301.
[6] P.P. Sahay, S. Tewari, S. Jha, M. Shamsuddin, J. Mater. Sci. 40 (2005) 4791.
[7] F.C. Lin, Y. Takao, Y. Shimizu, M. Egshiro, Sens. Actuators B 24–25 (1995) 843.
[8] C.T. Troy, Photon. Spectra 31 (1997) 34.
[9] M. Krunks, E. Mellikov, Thin Solid Films 33 (1995) 270.
[10] J.A. Aranovich, D. Golmaya, A.L. Fahrenbruch, R.H. Bube, J. Appl. Phys. 51 (1980) 4260.
[11] P.P. Sahay, J. Mater. Sci. 40 (2005) 4383.
[12] M.H. Huang, S. Mao, H. Feick, H. Yan, Y. Wu, H. Kind, E. Weber, R. Russo, P. Yang, Science 292 (2001) 1897.
[13] C.J. Lee, T.J. Lee, S.C. Lyu, Y. Zhang, H. Ruh, H. Lee, Appl. Phys. Lett. 81 (2002) 3648.
[14] Y.I. Alivov, E.V. Kalinina, A.E. Cherenkov, D.C. Look, B.M. Ataev, A.K. Omaev, M.V. Chukichev, D.M. Bagnall, Appl. Phys. Lett. 83 (2003) 4719.
[15] A. Mang, K. Reimann, St. Rübenacke, Solid State Commun. 94 (1995) 251.
[16] S.J. Young, L.W. Ji, S.J. Chang, Y.K. Su, J. Crystal Growth 293 (2006) 43.
[17] H. Kato, M. Sano, K. Miyanoto, T. Yao, Jpn. J. Appl. Phys. 42 (2003) L1002.
[18] T.M. Barnes, J. Leaf, S. Hand, C. Fry, C.A. Wolden, J. Appl. Phys. 96 (2004) 7036.
[19] J.A. Rodriguez, T. Jirsak, J. Dvorak, S. Sambasivan, D.J. Fischer, J. Phys. Chem. B 104 (2000) 319.
[20] K.L. Chopra, S. Major, D.K. Pandya, Thin Solid Films 102 (1983) 1.
[21] S. Major, A. Banerjee, K.L. Chopra, Thin Solid Films 108 (1983) 333–340.
[22] A. Ishizumi, Y. Takahashi, A. Yamamotoa, Y. Kanemitsu, Mater. Sci. Eng. B 146 (2008) 212.
[23] K. Hauffe, A.L. Vierk, J. Phys. Chem. 196 (1950) 160.
[24] C. Wagner, J. Chem. Phys. 18 (1950) 69.
[25] A.F. Aktaruzzaman, G.L. Sharma, L.K. Malhotra, Thin Solid Films 198 (1991) 67.
[26] A. Setiawan, Z. Vashaei, M.W. Cho, T. Yao, H. Kato, M. Sano, K. Miyamoto, I. Yonenaga, H.J. Ko, J. Appl. Phys. 96 (2004) 3763.
[27] Y. Sato, S. Sati, Thin Solid Films 281 (1996) 445.
[28] W.-C. Shih, M.-S. Wu, J. Crystal Growth 137 (1994) 319.
[29] D. Berhanu, D.S. Boyle, K. Govender, P. Brien, J. Mater. Sci. Mater. Elect. 14 (2003) 579.
[30] A.P. Roth, D.F. Williams, J. Electrochem. Soc. 128 (1981) 2684.
[31] F. Chaabouni, M. Abaab, B. Rezig, Mater. Sci. Eng. B 109 (2004) 236.
[32] Y. Natsume, H. Sakata, T. Hirayama, H. Yanagida, J. Appl. Phys. 72 (1992) 4204.
[33] E.M. Kaidashev, M. Lorenz, H. von Wenckstern, A. Rahm, H.C. Semmelhack, K.H. Han, G. Benndorf, C. Bundesmann, H. Hochmuth, M. Grundmann, Appl. Phys. Lett. 82 (2003) 3901.
[34] V. Musat, B. Teixeira, E. Fortunato, R.C.C. Monteiro, Thin Solid Films 502 (2006) 219.
[35] H.W. Lee, B.G. Choi, K.B. Shim, Y.J. Oh, J. Ceram. Process. Res. 6 (2005) 52.
[36] Y. Natsume, H. Sakata, Thin Solid Films 372 (2000) 30.
[37] D.W. Lane, J.A. Coath, K.D. Rogers, B.J. Hunnikin, H.S. Beldon, Thin Solid Films 221 (1992) 262.
[38] K.G. Benny Joseph, P.K. Gopchandran, J.J. Manoj, Abraham, V.K. Peter Koshy, Vaidyan, Indian J. Phys. A72 (1998) 99.
[39] M. Jin, M.H. Lei, L. Shu-Ying, J. Vac. Sci. Technol. A 13 (1995) 92.
[40] S.C. Erwin, L. Zu, M.I. Haftel, Al.L. Efros, T.A. Kennedy, D.J. Norris, Nature 436 (2005) 91.
[41] G.M. Dalpin, J.R. Chelikowsky, Phys. Rev. Lett. 96 (2006) 226802.
[42] D.J. Norris, N. Yao, F.T. Charnock, T.A. Kennedy, Nano Letters 1 (2001) 3.
[43] A. Ishizumi, C.W. White, Y. Kanemitsu, Appl. Phys. Lett. 84 (2004) 2397.
[44] Y. Kanemitsu, H. Matsubara, C.W. White, Appl. Phys. Lett. 81 (2002) 535.
[45] A. Ishizumi, Y. Kanemitsu, Appl. Phys. Lett. 86 (2005) 253106.
[46] A. Ishizumi, Y. Taguchi, A. Yamamoto, Y. Kanemitsu, Thin Solid Films 486 (2005) 50.
[47] P.V. Radovanovic, N.S. Norberg, K.E. McNally, D.R. Gamelin, J. Am. Chem. Soc. 124 (2002) 15192.
[48] K.R. Kittilstved, J. Zhao, W.K. Liu, J.D. Bryan, D.A. Schwartz, D.R. Gamelin, Appl. Phys. Lett. 89 (2006) 062510.
[49] B.D. Cullity, S.R. Stock, Elements of X-ray diffraction, 3rd edition, Prentice Hall, 2001.
[50] R.B. Bylsma, W.M. Becker, J. Kossut, U. Debska, Phys. Rev. B 33 (1986) 8207.
[51] C.V. Gopal Reddy, W. Cao, O.K. Tan, W. Zhu, S.A. Akbar, Sens. Activators B13 (2003) 115.